◆ Human Brain Mapping 35:4267–4281 (2014) ◆

TECHNICAL REPORT

Stimulus-Evoked Potentials Contribute to Map the Epileptogenic Zone During Stereo-EEG Presurgical Monitoring

Davide Boido,[1] Dimos Kapetis,[2] Vadym Gnatkovsky,[1] Chiara Pastori,[1] Barbara Galbardi,[2] Ivana Sartori,[3] Laura Tassi,[3] Francesco Cardinale,[3] Stefano Francione,[3] and Marco de Curtis[1]*

[1]*Experimental Neurophysiology and Epileptology Unit, Fondazione Istituto Neurologico Carlo Besta, Milano, Italy*
[2]*Bioinformatics Unit of Scientific Direction, Fondazione Istituto Neurologico Carlo Besta, Milano, Italy*
[3]*Claudio Munari Epilepsy Surgery Center, Ospedale Niguarda Cà Granda, Milano, Italy*

Abstract: Presurgical monitoring with intracerebral electrodes in patients with drug-resistant focal epilepsy represents a standard invasive procedure to localize the sites of seizures origin, defined as the epileptogenic zone (EZ). During presurgical evaluation, intracerebral single-pulse electrical stimulation (SPES) is performed to define the boundaries of eloquent areas and to evoke seizure-associated symptoms. Extensive intracranial exploration and stimulation generate a large dataset on brain connectivity that can be used to improve EZ detection and to understand the organization of the human epileptic brain. We developed a protocol to analyse field responses evoked by intracranial stimulation. Intracerebral recordings were performed with 105–162 recording sites positioned in fronto-temporal regions in 12 patients with pharmacoresistant focal epilepsy. Recording sites were used for bipolar SPES at 1 Hz. Reproducible early and late phases (<60 ms and 60–500 ms from stimulus artefact, respectively) were identified on averaged evoked responses. Phase 1 and 2 responses recorded at all and each recording sites were plotted on a 3D brain reconstructions. Based on connectivity properties, electrode contacts were primarily identified as receivers, mainly activators or bidirectional. We used connectivity patterns to construct networks and applied cluster partitioning to study the proprieties between potentials evoked/stimulated in different regions. We demonstrate that bidirectional connectivity during phase 1 is a prevalent feature that characterize contacts included in the EZ. This study shows that the application of an analytical protocol on intracerebral stimulus-evoked recordings provides useful information that may contribute to EZ detection and to the management of surgical-remediable epilepsies. *Hum Brain Mapp 35:4267–4281, 2014.* © **2014 Wiley Periodicals, Inc.**

Contract grant sponsor: Italian Health Ministry (Ricerca Corrente and Grant Giovani Ricercatori RF); Contract grant number: 114–2008; Contract grant sponsor: ERANET-NEURON project (2-p imaging).

*Correspondence to: Marco de Curtis, Experimental Neurophysiology and Epileptology Unit, Fondazione Istituto Neurologico, Milano, Italy. E-mail: decurtis@istituto-besta.it

Received for publication 20 September 2013; Revised 3 February 2014; Accepted 18 March 2014.
DOI 10.1002/hbm.22516
Published online 4 April 2014 in Wiley Online Library (wileyonlinelibrary.com).

Key words: epileptogenic zone; early propagation zone; magnetic resonance imaging; stereo electroencephalogram; single-pulse electrical stimulation

INTRODUCTION

Surgery resection of pathological tissue represents a major advancement for the cure of pharmaco-resistant focal epilepsy [see Engel, 2013; Scheffer and Mullen, 2013; Wiebe and Jette, 2012; Wiebe et al., 2001]. The identification of the epileptogenic region is not always trivial, particularly in cases with negative neuroimaging or when the epileptogenic area is in proximity to eloquent brain structures. For these patients, the recording of the stereo-electroencephalogram (SEEG) using intracerebral depth electrodes combined with video monitoring is a valid support for the identification of the epileptogenic zone (EZ) [Cossu et al., 2005; Talairach et al., 1974].

Patients are subjected to SEEG recordings for several days, to acquire the necessary information to assess the zone of seizure initiation and propagation and the extension of the seizure network. Several groups have developed computer-assisted analysis for the identification of the EZ and the seizure onset zone [Andrzejak et al., 2006; Bartolomei et al., 2008; Crepon et al., 2010; David et al., 2011; Gnatkovsky et al., 2011]. Computer-assisted analysis is useful to define the EZ with objective criteria, and is also suitable to extract the precious information in a unique circumstance, during which a direct window to the (pathological) generators of human brain activity is available.

To improve the identification of brain structures involved in seizure generation and their functions, electrical stimulations of the implanted electrodes are performed. High frequency trains of stimuli at 50 Hz and single pulse electrical stimulations (SPES) at 1 Hz delivered at electrode contacts close to or within the putative EZ are useful to elicit either seizure-related symptoms during the SEEG recording session, and are also used to define the boundaries of eloquent cortical areas [Bartolomei et al., 2004; David et al., 2013; Kahane et al., 2003; Lachaux et al., 2007; Lesser et al., 1987; Luders et al., 1986; Ojemann et al., 1989; Penfield and Jasper, 1954]. Previous studies have analysed the features of SPES-evoked responses to evaluate the epileptogenic area [Valentín et al., 2002] and identified delayed responses as intracranial markers of EZ in adults [Valentín et al., 2002, 2005] and children [Flanagan et al., 2009] with pharmacoresistant focal epilepsies. Moreover, SPES can be used to study human cortical connectivity in both epileptic [David et al., 2008; Matsumoto, 2004; van't Klooster et al., 2011] and physiological networks [Catenoix et al., 2011; David et al., 2013].

In this report, we quantitatively measured the effect of SPES delivered to implanted contacts, considering the activation brought and received by each recording contact in a population of patients explored with SEEG during pre-surgical monitoring. The large amount of data recorded during SPES protocols hinders the extraction of valuable information on the effect of single stimulation site in all SEEG traces. The aim of this study was to develop a protocol to organize SPES-evoked responses as functional maps and ascribe these maps to the epileptogenic tissue and the surrounding cortical regions.

METHODS

Stereo-EEG Recordings: Materials and Equipment

Twelve adult patients with pharmacoresistant partial epilepsy of heterogeneous etiologies submitted to SEEG exploration in fronto-temporal regions were examined (Table I). The recording contacts located either in the EZ (defined as the region of initiation and early propagation of seizures), or in the surrounding early-propagation zone (EPZ; defined as the area of early propagation of the ictal discharge) or in the normal tissue that surrounds these areas (not-epileptogenic healthy tissue) were identified for each patient by expert clinical neurophysiologists (SF, IS, and LT). Electrodes included in the EZ were defined by a time onset of fast activity included in the first second of the seizure. Electrodes in which fast activity was observed after 1 s were identified as EPZ. Patients were implanted with depth electrodes for pre-surgical evaluation, according to the stereotactic method [Cossu et al., 2005; Munari et al., 1993; Talairach et al., 1974]. Twelve to sixteen intracerebral multichannel electrodes (Dixi Medical, France and ALCIS, France), each carrying 5–18 contacts (length, 2 mm, diameter, 0.8 mm; 1.5 mm apart) were implanted, for a total number of 105–162 recording sites per patient. SEEG recordings with 0.016–300 Hz band-pass filter were performed using Neurofax EEG-1100 system (Nihon Kohden, Tokyo, Japan) at 1 kHz sampling rate and 16-bit resolution.

Based on the preoperative MR data and post-implantation computer tomography scans, image fusion was performed to locate each lead on the recording electrode trajectory (Fig. 1A). Intracerebral SPES were performed as part of the usual clinical assessment to locate both the epileptogenic and eloquent regions. Thirty bipolar 2 ms pulses of 5 mA intensity (lowered to 1–3 mA for SPES in both hippocampus and motor cortex) at 1 Hz were applied to couples of contiguous contacts on the same electrode shaft [Cardinale et al., 2013; Munari et al., 1993; Nathan et al., 1993]. SPES never triggered either epileptic seizure or sustained afterdischarges. All patients were surgically treated and EZs were confirmed both by

TABLE I. Patients data

Patient	Sex	Age at seizure onset	Age at sEEG	Electrodes/ recording sites	Postsurgical follow-up (months)	Seizure outcome (Engel scale)
1	M	22	28	12/144	16	Ib
2	F	1	26	15/158	24	Ia
3	M	12	32	15/158	24	Ia
4	M	4	25	13/105	30	Ia
5	M	5	17	14/161	10	IIIa
6	F	6	16	15/160	30	Ia
7	M	11	33	13/120	11	IIa
8	M	4	19	12/162	26	Ia
9	F	8	29	14/114	14	Ia
10	M	1	39	15/136	23	Ia
11	F	13	36	16/143	59	Ia
12	M	17	27	13/118	4	Ia

The number of electrodes implanted for SEEG monitoring and the total number of contacts are indicated.

histological examination of the resected tissue and by the postsurgical outcome. Seizure outcome was Engel scale Ia/b in 10 out of 12 patients (II and III a for patients 7 and 5, respectively; Engel, 1993). Postsurgical follow-up ranged between 4 and 59 months (see Table I).

Electrophysiological Data Analysis and Representation

SEEG data obtained during SPESs were acquired using custom-made software developed in LabView (National Instruments, Austin, TX; Fig. 1B). Trace segments of 600 ms (100 ms pre- and 500 ms post-stimulus; Fig. 1B) for all responses evoked by 1 Hz SPES were averaged for each stimulation site. Bipolar montages between contiguous recording sites were utilized to highlight local activations and to subtract passive volume-conducted components. Averaged SPES-evoked responses showed an early (2–60 ms) and a late (60–500 ms) principal components identified as phase 1 and 2, respectively (Fig. 1C,D). Reliability of SPES-evoked responses was evaluated by calculating a variability index on each average response, computed as the ratio between the summation of the standard deviations and the summation of the averaged points of each response, normalized for the number of points. Averaged responses with variability index values >0.1 were excluded from the analysis. Normalized areas (integral) subtended in the trace were calculated for the two phases. The absolute integral values were calculated, regardless the positive or negative signs of the potential. Recording sites in which SPES induced no responses were excluded from further analysis. For each stimulation, we classified the recording contacts as active and not active on the basis of two thresholds applied to the response peak amplitude and normalized area, respectively. The incrementally sorted values of both parameters were plotted and thresholds were automatically suggested by the program in order to exclude the responses with lowest values. The two thresholds could be manually adjusted, and were usually set either at 1/10 of the maximum value or at the value from which the distribution clearly increased its slope. Active contacts were the ones above at least one of the two thresholds. Saturating or noisy contacts were manually removed by visual inspection.

Based on contact spatial coordinates calculated from MR sequences, a three-dimensional (3D) map of the position of the implanted electrodes was created in a virtual 3D space (Fig. 2A,B) and subsequently transposed on MR reconstruction of the patient brain (Fig. 1A). Each recording site was represented by a dot that showed a size proportional to the values of averaged integrals. Recording sites in which no supra-threshold responses were measured are illustrated with small size gray dots. The interpretation of color codes and sizes of dots are defined in the Results section. Statistical evaluation was performed using one-way ANOVA with Tukey's post-hoc test. An a priori 95% confidence was set as sufficient to assess statistically significant differences; higher significance values are reported in the text and figure legends.

Network Connectivity Maps and Graph Partitioning

To understand the topological relationship between the recording contacts, we constructed connectivity network maps using Cytoscape 2.4.1 software (http://www.cytoscape.org [Shannon, 2003] see Results). The partition of the network into overlapping clusters of highly interconnected contacts was performed using the ClusterONE plugin (Clustering with Overlapping Neighborhood Expansion). ClusterONE algorithm aims to discover densily connected subgraphs over the network by growing dense regions out of small seeds given by a quality function of cohesiveness which measures how likely it is for a group of vertices to form a dense cluster [Nepusz et al., 2012] (Supporting Information - ClusterONE algorithm). This approach lacks

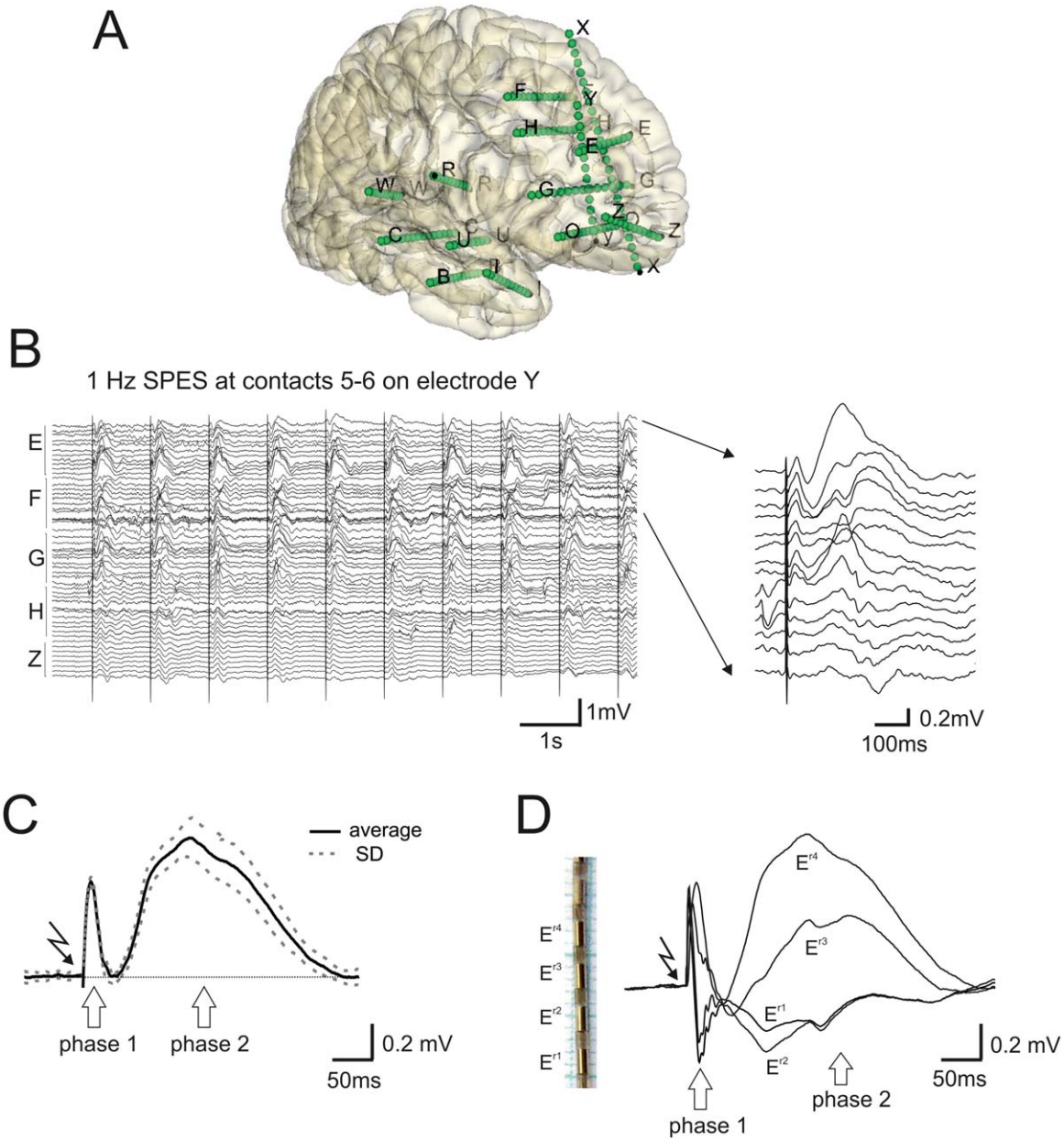

Figure 1.

SEEG data analysis. **A:** 3D reconstruction of intracerebral electrodes tracks on MR-CT fusion images of patient 9 (see Table I). Letters mark different electrodes. Single recording leads are presented as dots. **B:** Raw bipolar signals recorded from electrodes E, F, G, H, and Z in the same patient shown in A, during a 1 Hz SPES delivered at electrode Y. Expansion of traces recorded with electrodes E and F are shown on the right. **C:** Average (and SD: dotted line) of 30 SPES at 1 Hz delivered at electrode Y in patient 3. Early phase 1 (<60 ms) and a late phase 2 (60–500 ms) are clearly identified. The stimulus artifact is indicated with a bolt symbol. **D:** Averaged bipolar potentials recorded using four consecutive recording sites on electrode E. Four recording leads are illustrated as examples on an electrode microphotograph. [Color figure can be viewed in the online issue, which is available at wileyonlinelibrary.com.]

any bias due to subjective interpretations of the maps, fostered by statistical significances. No a priori restriction on both the number and the size of the clusters was imposed on the unsupervised clustering algorithm and therefore no information regarding the pathological position or brain region of each contact was provided. Statistical

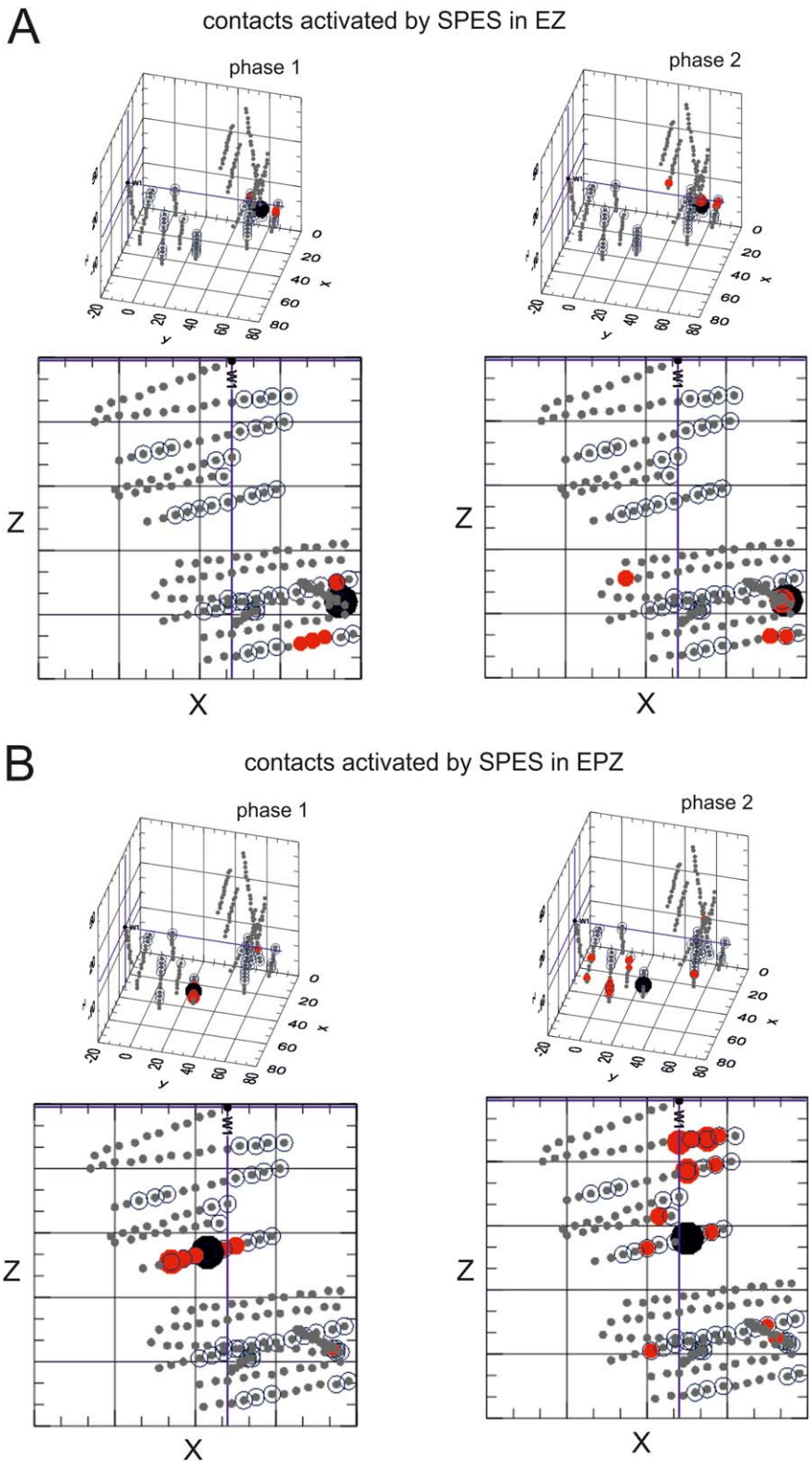

Figure 2.

Distribution of SPES-evoked responses. **A:** Amplitude of suprathreshold average integral amplitudes recorded in all SEEG recording sites during phase 1 (left panel) and phase 2 (right panel), following stimulation of a contact (large black spot) positioned in the EZ (dotted spheres). The size of red dots is proportional to the response amplitude normalized with respect to maximal responses. 3D plots with corresponding horizontal projections (bottom) **B:** Amplitude response plots as in A, following stimulation of a contact positioned in the EPZ. 3D plots with corresponding horizontal projections (bottom). [Color figure can be viewed in the online issue, which is available at wileyonlinelibrary.com.]

significance of each cluster is assigned using a one-sided Mann-Whitney U test performed on the number of internal and external boundary edges. The internal boundary edge was defined between the cluster node and the node within the cluster, while the external boundary edge was defined between the cluster node and the node outside the cluster. The clusters were visualized using Cytoscape's Organic layout, which is a force-directed layout algorithm similar to the Fruchterman-Reingold approach [Fruchterman and Reingold, 1991]. NAViGaTOR software (http://ophid.utoronto.ca/navigator, ver. 2.1.14) was used to visualize 3D connectivity maps. Results were further validated by Markov clustering algorithm (not shown). All clusters with $P < 0.05$ were extracted from the network according to density, quality and internal/external edge parameters and were identified as included in either EZ or EPZ or healthy tissue. The clusters were defined as belonging to either EZ or EPZ when more than 30% contacts were included in EZ or EPZ, respectively, according to surgical planning and postsurgical outcome.

RESULTS

Characteristics of SPES-Evoked Potentials

Analyses of SPES-evoked responses in different patients consistently identified early phase 1 and late phase 2 (Fig. 1B–D) [see also Kubota et al., 2013]. The integral values of phase 1 and phase 2 were measured in all recorded sites following SPES in all contacts and were plotted on 3D reconstructions of the brains of patients. Figure 2 illustrates a representative example of supra-threshold averaged integral responses (red dots) in phase 1 (left panels) and phase 2 (right panels) evoked by SPES delivered on contacts included in the EZ (marked by the large black dots in Fig. 2A) and EPZ (large black dot in Fig. 2B) in a single patient (Patient 9; data from the same patient are shown in Figs. 3, 5, and 6). Contacts retrospectively included in both EZ and EPZ are represented as outlined spots, which are more evident in the horizontal projections under each 3D plot. The same findings could be illustrated in a complementary manner, by representing stimulation sites that induce a response at a single recording contact (not shown). This process generated for each patient more than 10.000 computed values, which are difficult to summarize and visualize as functional maps.

Protocol Analysis of SPES-Evoked Data

To improve the reading of SPES-evoked data, each recording was classified either as a prevalent activator that induces evoked responses in other contacts, or as a prevalent receiver from other stimulated contacts (Fig. 3). Bidirectional contacts that received from the same activated contacts were also identified. The inclusion of a contact in one of the 3 categories was assessed using the following activating/receiving index (AR index):

$$\text{AR-INDEX} = \begin{cases} \dfrac{N_{\text{a.ed}} - N_{\text{bidir}}}{N_{\text{a.ing}} - N_{\text{bidir}}}, & \text{if } N_{\text{a.ed}} \leq N_{\text{a.ing}} \\ \dfrac{N_{\text{a.ing}} - N_{\text{bidir}}}{N_{\text{a.ed}} - N_{\text{bidir}}}, & \text{if } N_{\text{a.ed}} > N_{\text{a.ing}} \end{cases}$$

where $N_{a.ed}$ is the number of activated contacts and $N_{a.ing}$ is the number of activating contacts.

Using the 3D coordinates of each contact, plots of AR-indices for main activator contacts (red dots in Fig. 3) and primary receiver contacts (blue dots in Fig. 3) for both phases 1 and 2 (phase 2 not shown) and their spatial distribution and correlation with the EZ and EPZ (contacts outlined by the dotted sphere) were characterized. Notably, not all recording contacts are stimulated in clinical practice, thus the number of potentially activated contacts is consistently higher than or equal to the number of activating contacts. A threshold set to zero defines pure activators/receivers. The distribution of the bidirectional contacts in both phases was also evaluated (Fig. 3, phase 1 only), applying a threshold on the number of bidirectional connections.

The quantification of activator or receiver contacts performed in the cohort of 12 patients showed no prevalent distribution pattern in EZ, in EPZ or the peri-EZ-EPZ tissue for both phases (Fig. 4A–D). Neither the averaged AR-index nor the percentage of activators/receivers revealed statistically significant differences between the two phases in different areas. We did not observe evident correlations between activators or receivers and the EZ/EPZ when this analysis was repeated after varying AR index thresholds from 0 to 0.5. AR-index for activators and receivers was computed for each patient and illustrated with continuous gray lines superimposed onto average histograms plots of Figure 4A–D. The single patient data confirmed that EZ, EPZ, and the surrounding non-epileptogenic healthy tissue contain similar numbers of activating and receiving contacts

Next, we evaluated bidirectional contacts inside and outside the pathological zones. The number of bidirectional connections varied from patient to patient, depending on the extension of the EZ and on the contact density positioned in the explored brain region (see Supporting Information Fig. 1A). To correct for this variability, we computed the average number of bidirectional connections of each stimulated contact, after dividing the average number of bidirectional connections in the healthy tissue. These values were subsequently averaged among patients (Fig. 4E,F). During phase 1 only, the normalized number of bidirectional contacts in the EZ was significantly higher than in the healthy tissue (one-way ANOVA, $P < 0.05$; Fig. 4E). The same statistical analysis was conducted on non-normalized values for bidirectional connections and the significance of the difference between EZ and healthy tissue was equally assessed (Supporting Information Fig. 1).

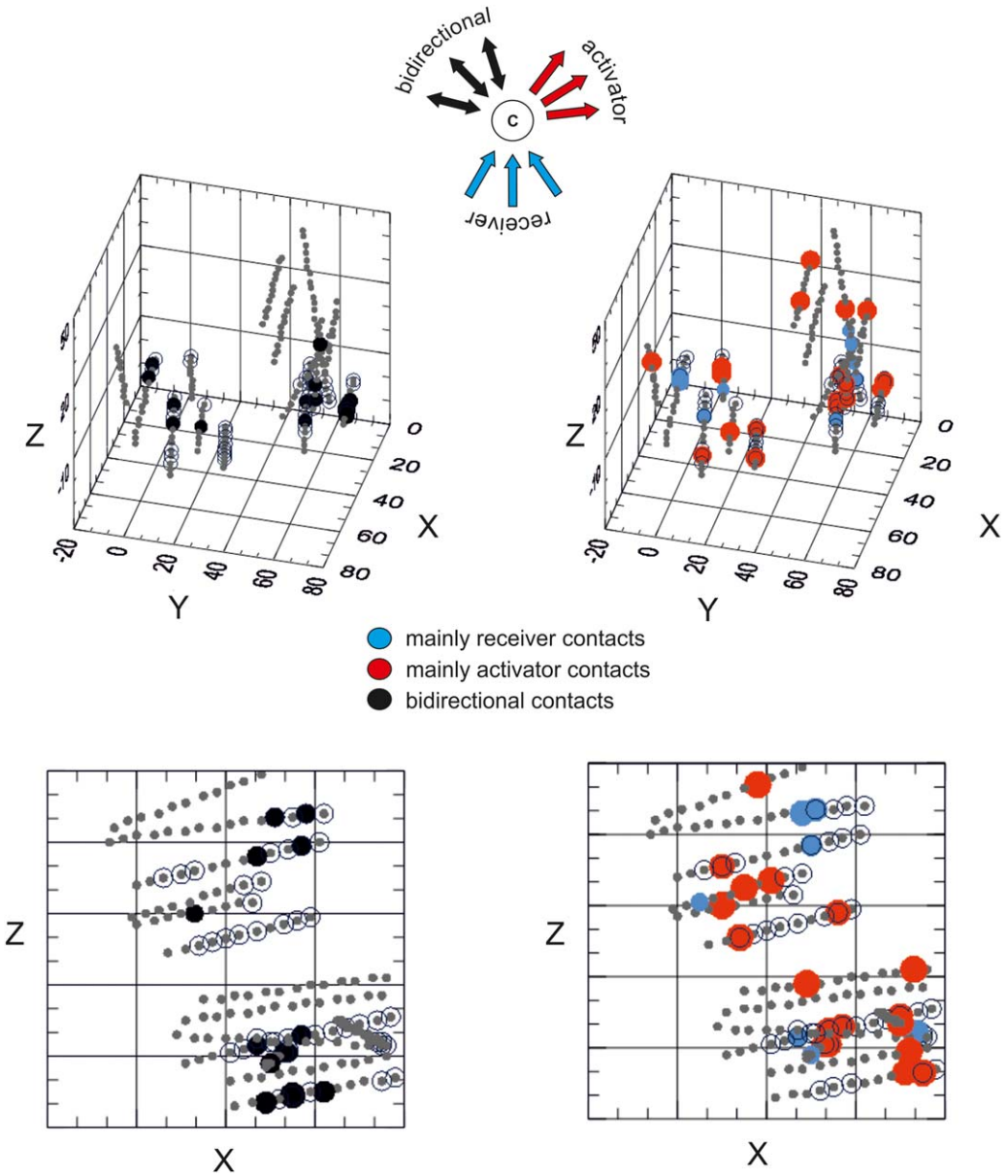

Figure 3.

Activating, receiving, and bidirectional connections. Schematic representation of a contact (center dot marked with a C) as mainly receiver of inputs from other contracts (blue arrows) or mainly activator of other contacts (red arrows) is shown on top. Bidirectional relationship between coupled receiving and activating contacts are represented by black arrows. On the left, a threshold based on the number of bidirectional contacts (>4) was used to illustrate the contacts with the highest number of bidirectional connections (black dots) during phase 1 in patient 9 on a 3D space in which the position of the electrodes is reconstructed based on MR coordinates (bottom, the horizontal projection). On the right a plot of the distribution of phases 1 contacts defined mainly as receiving (blue dots) and activating (red dots) after setting a threshold value of AR-index < 0.1 for the main activators and < 0.5 for the main receivers (see Methods) is shown for patient 9 (bottom, the horizontal projection). [Color figure can be viewed in the online issue, which is available at wileyonlinelibrary.com.]

We also computed the percentage of highly bidirectional contacts (with bidirectionality index higher than the average value of the healthy tissue) with respect to all contacts in pathological and normal tissues. In the EZ we observed only a trend for a higher probability of bidirectional connections in phase 1 (Fig. 4E,F). Bidirectionality evaluated

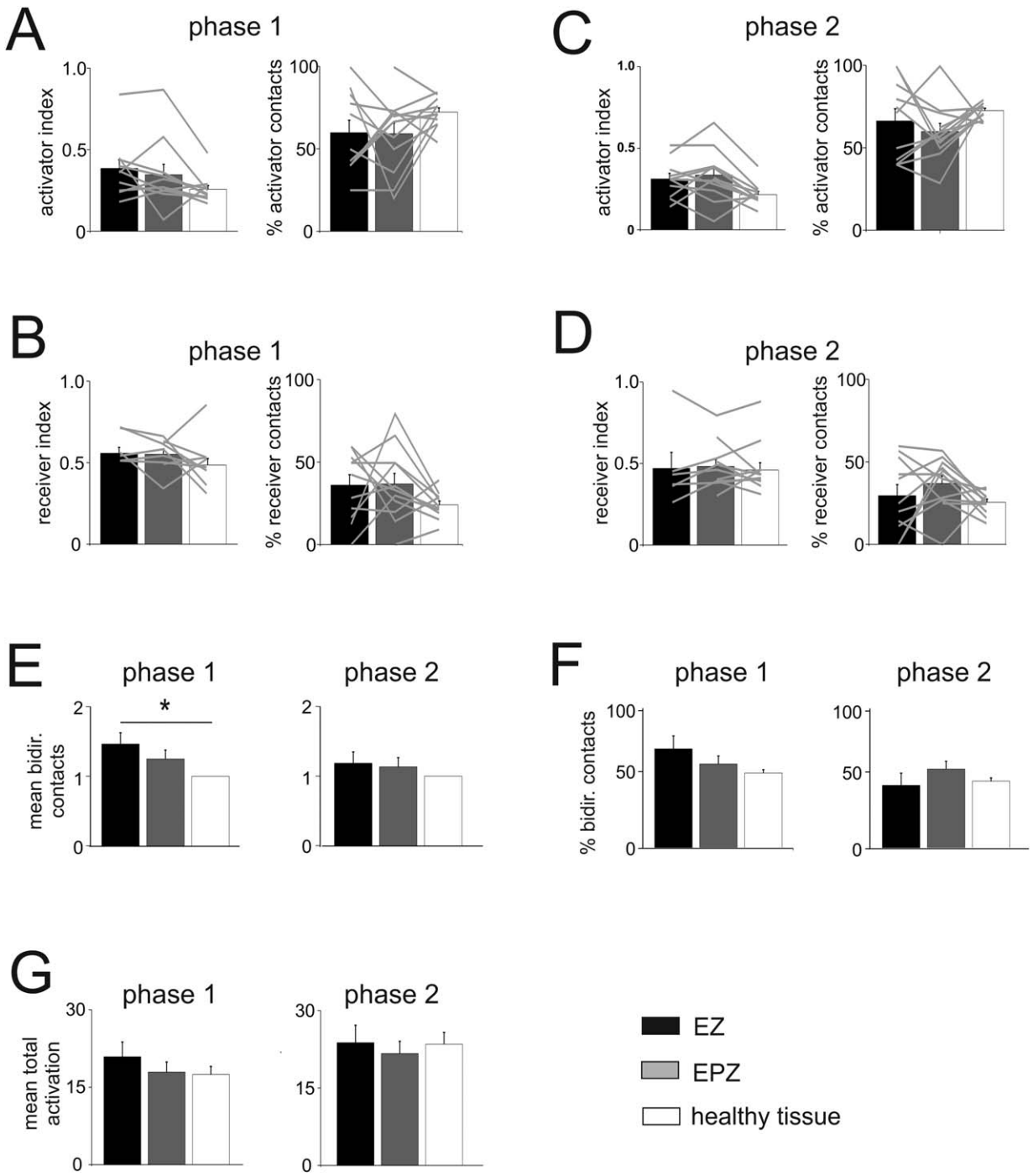

Figure 4.

Distribution of activating, receiving, and bidirectional connections. **A–D:** Average values of AR-index for mainly activator or receiver contacts and the percentage of activator and receiver contacts for phase 1 (A and B) and phase 2 (C and D) in EZ (black columns), EPZ (gray columns), and healthy tissue (white columns), calculated in 12 patients. Values from each patient are illustrated by light gray lines. **E:** Quantification of the average number of bidirectional connections in EZ and EPZ normalized to the mean number of bidirectional connection of the contacts in healthy tissue calculated for phase 1 (left) and phase 2 (right panel). **F:** Percentage of bidirectional connections in EZ and EPZ calculated for phase 1 (left) and phase 2 (right panel). The value of normalized bidirectionality and percentage beside the absolute number of mean bidirectional contacts from each patient are reported in Supporting Information Figure 1. **G:** The total activation is the summation of activated and activating contacts for each stimulated contact, minus the number of bidirectional connections, averaged with respect to the pathological and healthy regions. The absence of any statistical significance in this parameter let us reject the hypothesis of a bias on the activator or receptor behavior of each contact due to a higher number of activated/activating contacts.

in phase 2 did not reveal any significant correlation with pathological tissue (Fig. 4E,F). The sum of the number of activated and activating contacts could be a possible bias for bidirectionality values of each contact. Thus, we evaluated the mean total activation in the three zones for each patient in each phase and observed no significant differences (Fig. 4G). The data analysis subdivided for each patient is illustrated in detail in Supporting Information Figure 1B–D.

These findings demonstrate that bidirectional interactions are prevalent within the EZ when evaluated by analyzing SPES-evoked responses. This type of analysis is statistically relevant, but does not provide functional mapping of the explored brain areas easy to examine.

Network Connectivity Maps and Graph Partitioning

To study the spatial distribution of SPES-evoked functional interactions, we used a different approach based on bidimensional analysis of connections among contacts by force-directed graph algorithm [Fruchterman and Reingold, 1991].

The localization of the recording contacts in the pathological zone of Patient 9, indentified by clinicians is shown in Figure 5A; red dots for EZ, yellow dots for EPZ (note this colors notation will remain valid for the following figures and in the Supporting Information).

As illustrated in Figure 5B, the graphical representation of connectivity maps obtained with this procedure shows the distribution of contacts based on their interactions and topology in an artificial functional environment (see Methods). In these maps, the unidirectional and bidirectional connections (see contact B11 in the insert in Fig. 5, phase 1) are drawn in light blue and blue respectively. The topology of the maps depends on the pattern of connections. Maps of the two phases of the same patient might have different shapes, but the grouping of EZ-EPZ contacts with respect to the whole map is preserved across phases (Fig. 5B).

To organize the seeds of the network (contacts) into discrete modules based on their common interconnection patterns, we applied the graph-clustering algorithm ClusterONE. Among the set of extracted clusters (with significant P, see Methods), we observed clusters overlapping almost perfectly with one of the pathological zones (Fig. 6A–C), clusters identifying structures with known functional role (hippocampus, motor cortex, etc.) and clusters linking distant portions of the map (Fig. 6D). The clusters were analyzed during phase 1 and phase 2 in 12 patients. EZ- and EPZ-clusters were defined by the presence of more than 30% of the contacts in either the EZ or the EPZ zones (black and gray columns, respectively, in Fig. 7). Clusters that did not include EZ-EPZ contacts were identified as healthy tissue clusters (white columns in Fig. 7). A total of 10 and 12 EZ clusters were identified for phases 1 and 2, respectively, and 24 and 27 EPZ clusters were identified for phases 1 and 2, respectively. Moreover, 67 and 63 healthy tissue clusters were correspondingly identified in phases 1 and 2. The main percentage of EZ/EPZ contacts included in EZ/EPZ clusters was, respectively, $49 \pm 3\%$ and $49 \pm 3\%$ in phase 1 and $51 \pm 4\%$ and $44 \pm 2\%$ in phase 2. Hybrid clusters (with EZ/EPZ contacts $<30\%$) that did not obey these rules were discarded from the analysis. A small overlap in the connectivity clustering between the EZ and EPZ was observed. The percentage of EPZ contacts in EZ clusters was on average 9% for phase 1 and 5% for phase 2. The EZ contacts in EPZ clusters were 3 and 4% for phases 1 and 2 respectively, independently of the anatomical proximity of these two zones. Focusing only on phase 1, 75% (9/12) of the patients had at least 1 cluster of EZ or EPZ-type and 33% (4/12) had at least 1 cluster that included both EZ and EPZ, whereas 92% of patients (11/12) showed healthy tissue clusters. Similar results were obtained in the analysis of phase 2. The number of bidirectional connections was significantly higher in phase 1 EZ and EPZ clusters than in the nonepileptogenic clusters ($P < 0{,}001$ and $P < 0{,}05$, respectively, Fig. 7B). The significance of the bidirectional contacts in the EZ clusters confirmed the findings derived from single-contact analysis (Fig. 4E,F). Moreover, the cluster bidirectionality was also significantly higher in the EPZ compared with nonepileptogenic tissue.

Other parameters were computed on clusters, such as the ratio between the number of bidirectional and unidirectional connections (Fig. 7C) and the quality, which refers to the ratio between internal and external connections to the cluster (Fig. 7D). These parameters showed a general larger values for EZ compared with other regions, without statistical significance, with the exception of the ratio between bidirectional and unidirectional connections in EZ compared with EPZ during phase 2.

DISCUSSION

We developed a quantitative procedure to analyze data from electrical stimulation protocols performed during SEEG, and to extract potentially useful features that contribute to assess the characteristics of the epileptogenic brain regions in patients with focal pharmacoresistant epilepsy. We propose that it is feasible to compute and to interpret the massive amount of data obtained by considering responses recorded from all electrodes following bipolar SPES of all sites.

The first step to achieve this goal was to identify two principal phases of SPES-induced responses. The reliability of these responses over all recording contacts facilitated the computation of average values for each and all SPES. Previous reports indicated that cortico-cortical field responses evoked by local intracortical stimulation in different regions of the human cortical mantle are characterized by two major components [Enatsu et al., 2012; Kubota

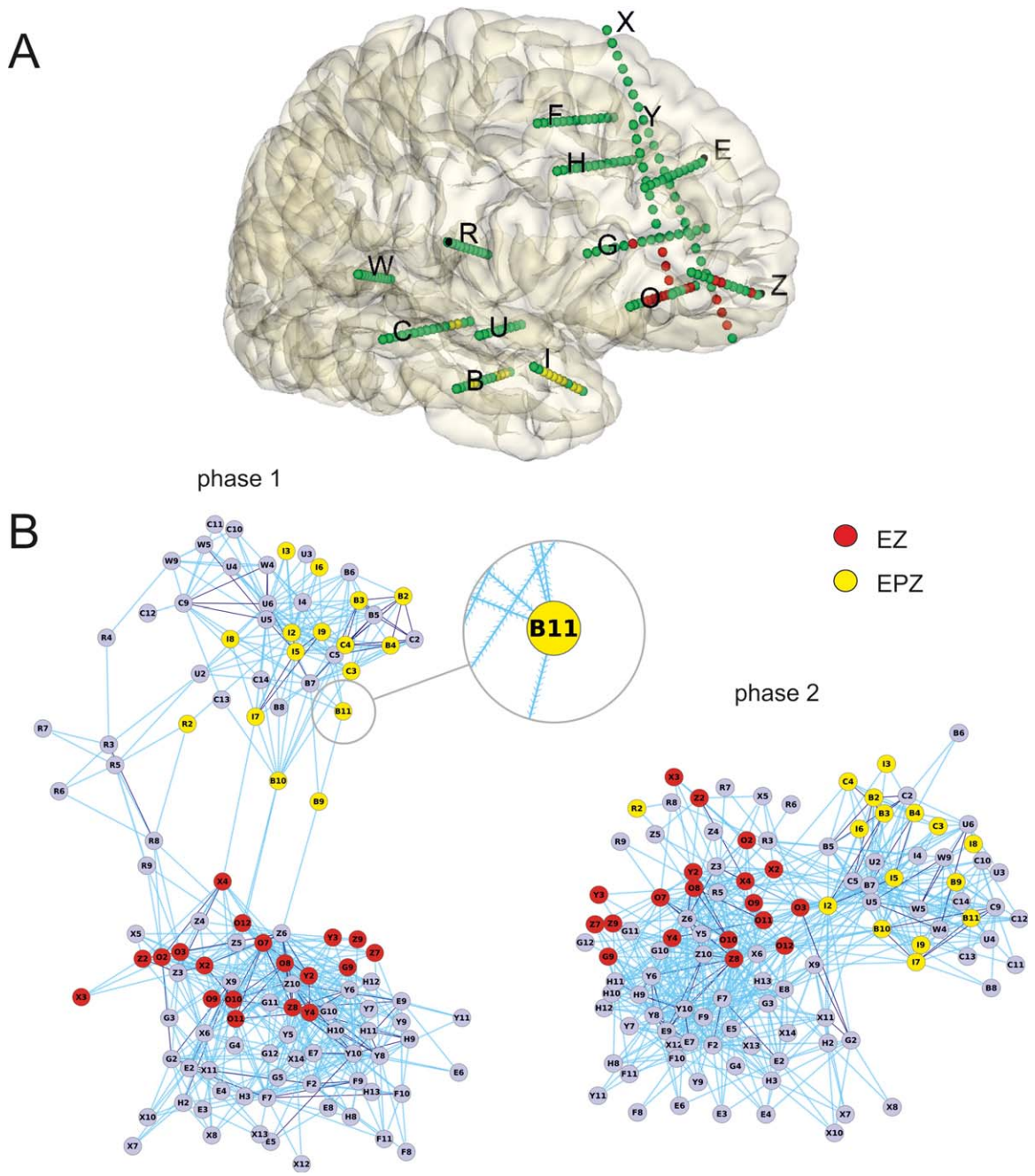

Figure 5.

A: Schema of the recording contacts inside the brain of patient 9; in red the contacts in the EZ and in yellow the ones in the EPZ. **B**: Two-dimensional connectivity maps based on the stimulated/activated contacts. Map of contact connectivity during phases 1 and 2 in patient 9, based on the analysis of averaged SPES-evoked responses. Separation between contacts was optimized using a force-directed layout [Fruchterman and Reingold, 1991]. Connections (light blue) with marked directions (see enlargement of B11 contact) originate from stimulated contacts and end on supra-threshold activated contacts. Purple lines represent bidirectional relationships between couples of contacts. EZ contacts (reported in red) are clustered separately from the EPZ contacts (in yellow) in this patient. Bridging links connect the two main groups of contacts both maps. The two main groups of contacts of phase 1 and 2 maps are all included in temporal lobe (upper and right groups in phase 1 and 2, respectively) and in frontal lobe (lower and right groups in phase 1 and 2, respectively). For phase 1, contacts interposed between the two groups represented intermediate structures between the two lobes: contacts R2 to R9 were located in the central operculum and contacts B9-B11 in the medium temporal gyrus.

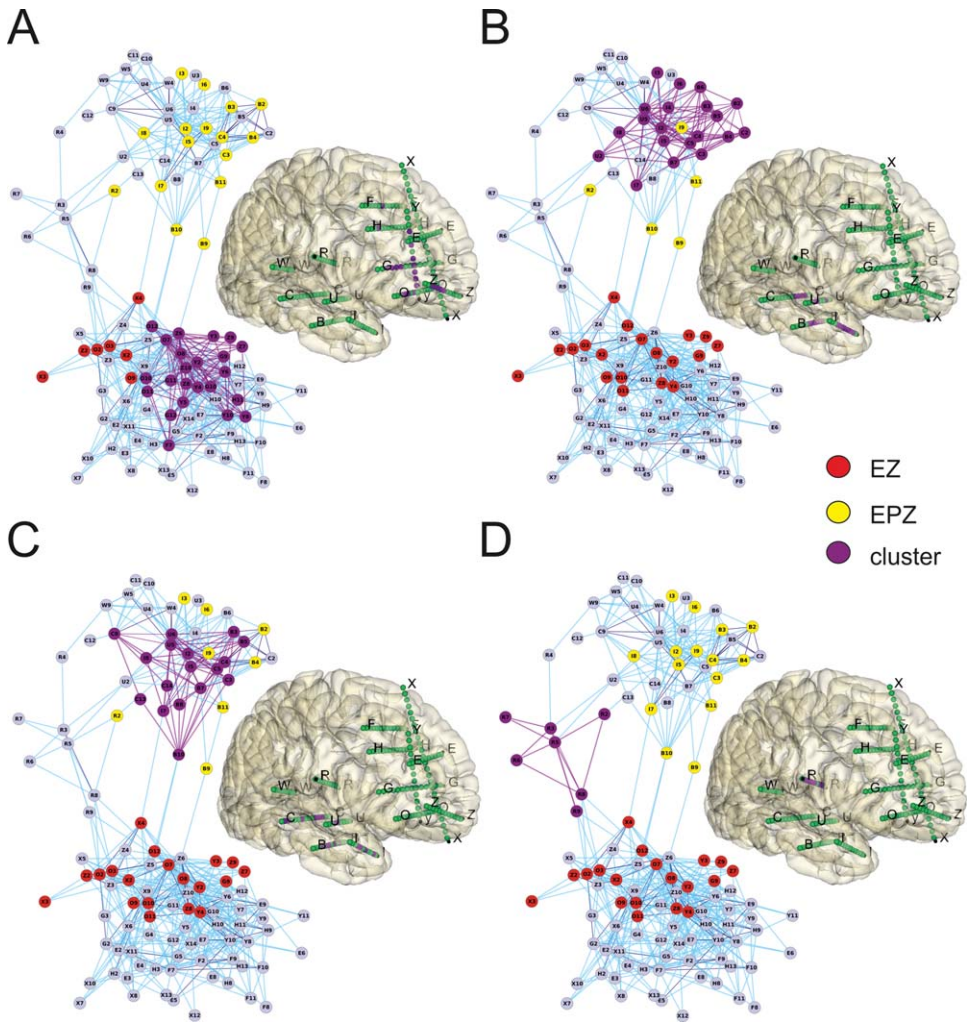

Figure 6.

Clustering of contacts analysed by connectivity features. ClusterONE network-clustering algorithm was applied to phase 1 connectivity 2D-map in the same patient 9 of Figure 5, to identify optimal clusters of contacts (in purple) sharing dense connection patterns. The contacts belonging to each cluster were also reported, with the same colour (on the side of each connectivity map), in the brain schema of the implanted electrodes of the patient. Red and yellow dots in the connectivity maps identify the EZ and the EPZ. The location of the clusters (purple contacts) in the 3D reconstruction of the patient brain is shown on the right in each panel. Cluster overlapping was permitted. **A**: Cluster matching with the EZ. **B** and **C**: Clusters included in the EPZ. **D**: Cluster matching with well-defined anatomical and functional healthy tissue structures that connect the temporal with the frontal lobe (opercular region).

et al., 2013; Nathan et al., 1993; Valentín et al., 2005; Wilson et al., 1990]. Phase 1 and phase 2 identified in our study respectively include the area underlying N1 and N2 waves of cortico-cortical evoked potentials described in the temporal region [Matsumoto, 2004]; these waves have peak latency of 20–35 ms and 110–170 ms. Phase 1 is due mainly to a population of postsynaptic excitatory potentials generated in cortical neurons in response to afferent cortical inputs [Douglas et al., 1995; Sugaya et al., 1964] that are possibly generated in deep cortical layers [Kumar and Huguenard, 2001; Mercer et al., 2005]. Phase 2 is either generated by recurrent inhibitory potentials that follow the direct excitation mediated by phase 1 [Silberberg and Markram, 2007], or can be sustained by polisynaptic cortico-cortical and/or cortico-subcortico-cortical excitatory circuits. Evidence for a contribute of polysynaptic (either inhibitory or excitatory) activation during phase 2 derives from paired-pulse stimulation protocols performed during intracranial exploration, by transcranial magnetic stimulation in humans [Ferreri et al., 2011; Wilson et al., 1998]

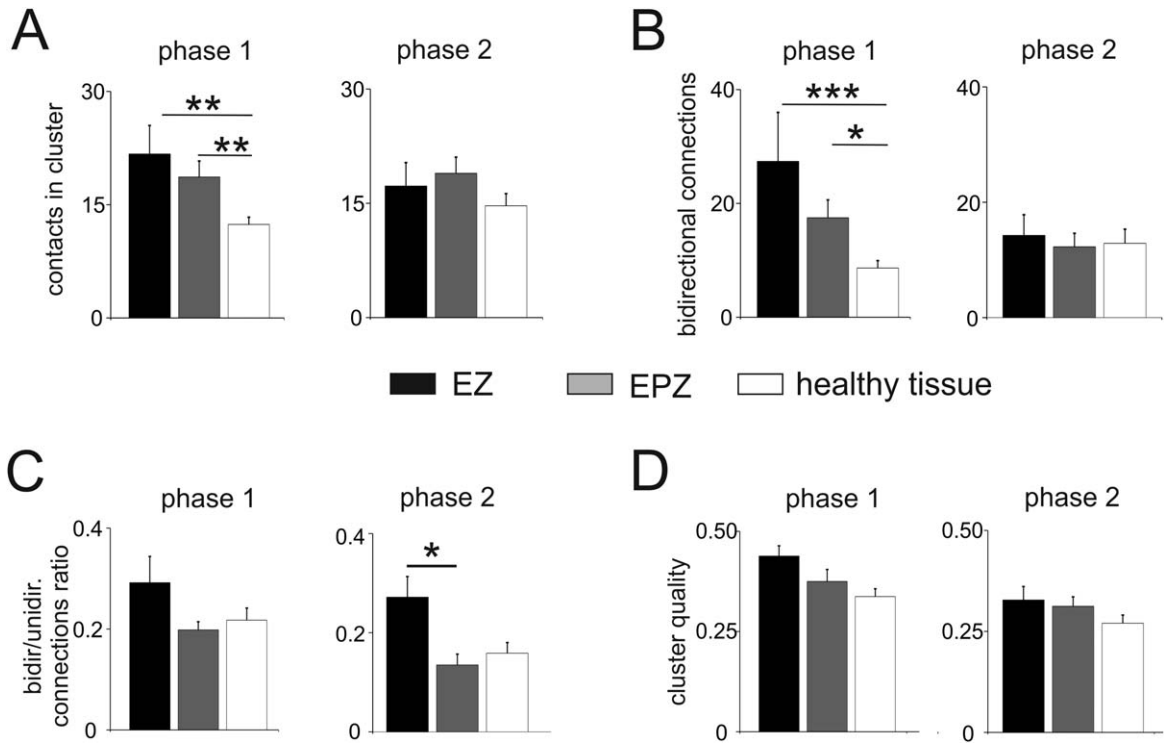

Figure 7.

Distribution of contact clusters. **A**: Mean number of contacts in EZ (black column), EPZ (gray column), and healthy tissue (white column) clusters during phases 1 and 2 calculate in all 12 patients. **B**: Number of bidirectional connections in EZ, EPZ, and healthy tissue clusters. **C**: Ratios between bidirectional and unidirectional connections for the two phases. **D**: Cluster quality feature comparison between EZ, EPZ, and healthy tissue clusters. Quality parameter represents a measure of cohesiveness, which assesses a well-defined cluster with many internal edges and few boundary edges. One-sided Mann-Whitney U test was used to determine the significance: ***= $P < 0{,}001$; ** = $P < 0{,}01$; *= $P < 0{,}05$.

and in experimental reports [Biella et al., 1996; Metherate and Ashe, 1994; Nathan and Lambert, 1991]. These studies demonstrated that the delayed component (lasting 300–600 ms) evoked by the second stimulus in a pair is abolished by inter-stimulus interval lower than 30 ms, suggesting a prevalent involvement of cortical recurrent inhibitory networks in its generation.

The computation of phase 1 and phase 2 average integral area dramatically decreased the data size to kilobytes and made it possible to represent the global effect of different stimulations in a 3D plot based on the exact spatial positions of the contacts obtained by MRI. Next, we introduced a further binary parameter by setting thresholds on the amplitude and area of the evoked responses to filter for non-relevant parameters and to highlight specific contacts. By considering only the active contacts, we were able to assess the activation propensity of each contact (main receiver, main activator, and bidirectional) and this approach further reduced the data set consenting of the analysis of reciprocal interactions between contacts, but did not allow for a clear mapping of these interactions. By quantitatively evaluating the propensity towards either activation or passive reception of individual SPES, we did not observe a significant preferred ability for activation or being activated in the contacts within the epileptic networks with respect to the surrounding healthy tissue. This suggests that neurons within the EZ (i) do not overrespond to an incoming cortical input and (ii) when stimulated do not generate a larger than normal response in surrounding healthy tissue. Bidirectionality of activation among contacts during phase 1 was a reliable indicator of the pathological tissue. Analyses of single contacts showed a significant higher number of bidirectional connections in the EZ with respect to the healthy tissue during phase 1, but not between EPZ and healthy tissue.

To interpret our data revealed by SPES, we integrated connection patterns into a global connectivity network map by applying graph clustering analysis derived from research fields such as molecular biology, social science, and statistical physics. Graph network theory has suggested several natural and local small-world properties typical of brain connectivity [Strogatz, 2001]. Network

clustering of SPES-evoked responses exploits connectivity maps to obtain a better understanding of the activation relationships among different cortical structures. A similar connectivity approach has been applied to evaluate synchronization properties of SEEG signal and the direction of the information flow in the epileptogenic region [Franaszczuk et al., 1994; Varotto et al., 2012; Wilke et al., 2010] or to functional MRI analysis [Pandit et al., 2013; Smith, 2002] and might contribute to functional connectomics evaluation of physiological and pathological brain networks [Alvisatos et al., 2012]. Connectivity mapping approach ensures contacts segregation in more densely connected clusters, thus allowing for an efficient information flow through the network that is otherwise hindered by visual analysis. Here, we took in advantage of the three different activation patterns (receiver, activator, and bidirectional) to construct network connectivity maps and to evaluate cluster proprieties of the EZ-EPZ and the healthy tissue. Exploiting the cluster parameters between EZ/EPZ against healthy tissue clusters, we revealed that highly dense clusters with more internal connections might reflect a pathological condition of the epileptogenic tissue. These characteristics are analogues to small-worlds phenomena with high clustering coefficients and high degree nodes, in which most nodes can be reached from every other node through a small number of hops or steps. Indeed, when we considered small assemblies of contacts sharing similar connectivity patterns instead of single contacts by connectivity maps and an automatic clustering algorithm, we obtained significant higher number of bidirectional connections in both EZ and EPZ clusters compared with pure healthy tissue clusters. These data confirmed and further extended the findings obtained with single correlation analysis, and strongly suggest that the epileptogenic area is formed by group of neurons that show a higher concentration of bidirectional connections with respect to cluster in close networks. High interconnectivity is particularly evident for interactions within the EZ and it is likely mediated by monosynaptic cortico-cortical interactions between groups of neurons, since this property is emerging exclusively for phase 1. This observation supports the assumption that phase 2 represents a local response (possibly inhibitory or polisynaptic) independent on cortico-cortical connectivity and generated by neuronal activation during the monosynaptic phase 1 component.

The possibility that connectivity clustering maps may highlight physiological networks among the different explored structures should be considered. In patients explored in the mesial temporal lobe, indeed, strong primary clustering within the hippocampal-entorhinal area were observed (see Supporting Information Fig. 2). In mesial temporal lobe exploration en passant to the EZ, such physiological, non-epileptic clusters were not included in the epileptogenic area. Nonclustering analysis of SPES-evoked responses was reported to study the connectivity of hippocampal afferent projections in patients during SEEG exploration [Catenoix et al., 2011]. It is interesting to notice that in the 4 patients explored with electrodes implanted in two different lobes (such as the patient illustrated in Figs. 5 and 6), clustering analysis during phase 1 revealed two separate groups of contacts connected by few interposed contacts. The 3D reconstruction of the position of the electrodes demonstrated that all contacts included in one of the two large map cluster are comprised in one lobe. Moreover, the contacts interposed between the two main groups are located in cortical areas that connect the two lobes (central operculum and medium temporal gyrus in patient 9; see figure legend of Fig. 6). This observation will need more accurate evaluation of multilobar explorations.

In conclusion, mapping bidirectionality features of SPES-evoked responses (mainly of early components correlated to phase 1) recorded during intracranial SEEG monitoring can be used to identify the EZ and may improve detection in those cases in which EZ is not easily defined by seizure patterns. Moreover, the recognition of pathological and healthy tissue clusters could facilitate the identification of the area of surgical resection.

REFERENCES

Alivisatos AP, Chun M, Church GM, Greenspan RJ, Roukes ML, Yuste R (2012) The brain activity map project and the challenge of functional connectomics. Neuron 74:970–974.

Andrzejak RG, Mormann F, Widman G, Kreuz T, Elger CE, Lehnertz K (2006): Improved spatial characterization of the epileptic brain by focusing on nonlinearity. Epilepsy Res 69:30–44.

Bartolomei, F, Wendling, F, Regis, J, Gavaret, M, Guye, M, Chauvel, P (2004): Pre-ictal synchronicity in limbic networks of mesial temporal lobe epilepsy. Epilepsy Res 61:89–104.

Bartolomei F, Chauvel P, Wendling F (2008): Epileptogenicity of brain structures in human temporal lobe epilepsy: Aa quantified study from intracerebral EEG. Brain 131:1818–1830.

Biella G, Panzica F, de Curtis M (1996): Interactions between associative synaptic potentials in the piriform cortex of the in vitro isolated guinea pig brain. Eur J Neurosci 8:1350–1357.

Cardinale F, Cossu M, Castana L, Casaceli G, Schiariti MP, Miserocchi A, Fuschillo D, Moscato A, Caborni C, Arnulfo, Lo Russo G (2013): Stereoelectroencephalography: Surgical methodology, safety, and stereotactic application accuracy in 500 procedures. Neurosurgery 72:353–366.

Catenoix H, Magnin M, Mauguière F, Ryvlin P (2011): Evoked potential study of hippocampal efferent projections in the human brain. J Clin Neurophysiol 122:2488–2497.

Cossu M, Cardinale F, Castana L, Citterio A, Francione S, Tassi L, Benabid AL, Lo Russo G (2005): Stereoelectroencephalography in the presurgical evaluation of focal epilepsy: A retrospective analysis of 215 procedures. Neurosurgery 57:706–718.

Crepon B, Navarro V, Hasboun D, Clemenceau S, Martinerie J, Baulac M, Adam C, Le Van Quyen, M (2010): Mapping interictal oscillations greater than 200 Hz recorded with intracranial macroelectrodes in human epilepsy. Brain 133:33–45.

David O, Woźniak A, Minotti L, Kahane P (2008): Preictal short-term plasticity induced by intracerebral 1 Hz stimulation. Neuroimage 39:1633–1646.

David O, Blauwblomme T, Job AS, Chabardes S, Hoffmann D, Minotti L, Kahane P (2011): Imaging the seizure onset zone with stereo-electroencephalography. Brain 134:2898–2911.

David O, Job A-S, De Palma L, Hoffmann D, Minotti L, Kahane P (2013): Probabilistic functional tractography of the human cortex. Neuroimage 1–42.

Douglas RJ, Koch C, Mahowald M, Martin KA, Suarez HH (1995): Recurrent excitation in neocortical circuits. Science 269:981–985.

Enatsu R, Jin K, Elwan S, Kubota Y, Piao Z, O'Connor T, Horning K, Burgess RC, Bingaman W, Nair DR (2012): Correlations between ictal propagation and response to electrical cortical stimulation: A cortico-cortical evoked potential study. Epilepsy Res 101:76–87.

Engel JJ (1993): Intracerebral recordings: Organization of the human epileptogenic region. J Clin Neurophysiol 10:90–98.

Engel JJ (2013): Progress in the field of epilepsy. Curr Opin Neurol 26:160–162.

Ferreri F, Pasqualetti P, Maatta S, Ponzo D, Ferrarelli F, Tononi G, Mervaala E, Miniussi C, Rossini PM (2011): Human brain connectivity during single and paired pulse transcranial magnetic stimulation. Neuroimage 54:90–102.

Flanagan D, Valentín A, García Seoane JJ, Alarcón G, Boyd SG (2009): Single-pulse electrical stimulation helps to identify epileptogenic cortex in children. Epilepsia 50:1793–1803.

Franaszczuk PJ, Bergey GK, Kaminski MJ (1994): Analysis of mesial temporal seizure onset and propagation using the directed transfer function method. Electroencephalogr Clin Neurophysiol 91:413–427.

Fruchterman TMJ, Reingold EM (1991): Graph Drawing by Force-Directed Placement. Software-Pract Exp 21:1129–1164.

Gnatkovsky V, Francione S, Cardinale F, Mai R, Tassi L, Lo Russo G, de Curtis M (2011): Identification of reproducible ictal patterns based on quantified frequency analysis of intracranial EEG signals. Epilepsia 52:477–488.

Kahane P, Hoffmann D, Minotti L, Berthoz A (2003): Reappraisal of the human vestibular cortex by cortical electrical stimulation study. Ann Neurol 54:615–624.

Kubota Y, Enatsu R, Gonzalez-Martinez J, Bulacio J, Mosher J, Burgess RC, Nair DR (2013): In vivo human hippocampal cingulate connectivity: A corticocortical evoked potentials (CCEPs) study. Clin Neurophysiol 124:1547–1556.

Kumar SS, Huguenard JR (2001): Properties of excitatory synaptic connections mediated by the corpus callosum in the developing rat neocortex. J Neurophysiol 86:2973–2985.

Lachaux J-P, Fonlupt P, Kahane P, Minotti L, Hoffmann D, Bertrand O, Baciu M (2007): Relationship between task-related gamma oscillations and BOLD signal: New insights from combined fMRI and intracranial EEG. Hum Brain Mapp 28:1368–1375.

Lesser RP, Luders H, Klem G, Dinner DS, Morris HH, Hahn JF, Wyllie E (1987): Extraoperative cortical functional localization in patients with epilepsy. J Clin Neurophysiol 4:27–53.

Luders H, Lesser RP, Hahn J, Dinner DS, Morris H, Resor S, Harrison M (1986): Basal temporal language area demonstrated by electrical stimulation. Neurology 36:505–510.

Matsumoto R (2004): Functional connectivity in the human language system: A cortico-cortical evoked potential study. Brain 127:2316–2330.

Mercer A, West DC, Morris OT, Kirchhecker S, Kerkhoff JE, Thomson AM (2005) Excitatory connections made by presynaptic cortico-cortical pyramidal cells in layer 6 of the neocortex. Cereb Cortex 15:1485–1496.

Metherate R, Ashe JH (1994): Facilitation of an NMDA receptor-mediated EPSP by paired-pulse stimulation in rat neocortex via depression of GABAergic IPSPs. J Physiol 481:331–348.

Munari C, Kahane P, Tassi L, Francione S, Hoffmann D, Lo Russo G, Benabid AL (1993): Intracerebral low frequency electrical stimulation: A new tool for the definition of the "epileptogenic area"? Acta Neurochir Suppl (Wien) 58:181–185.

Nathan T, Lambert JD (1991): Depression of the fast IPSP underlies paired-pulse facilitation in area CA1 of the rat hippocampus. J Neurophysiol 66:1704–1715.

Nathan SS, Sinha SR, Gordon B, Lesser RP, Thakor NV (1993): Determination of current density distributions generated by electrical stimulation of the human cerebral cortex. Electroencephalogr Clin Neurophysiol 86:183–192.

Nepusz T, Yu H, Paccanaro A (2012): Detecting overlapping protein complexes in protein-protein interaction networks. Nat Methods 9:471–472.

Ojemann G, Ojemann J, Lettich E, Berger M (1989): Cortical language localization in left, dominant hemisphere An electrical stimulation mapping investigation in 117 patients. J Neurosurgery 71:316–326.

Pandit AS, Robinson E, Aljabar P, Ball G, Gousias IS, Wang Z, Hajnal JV, Rueckert D, Counsell SJ, Montana G, Edwards AD: Whole-brain mapping of structural connectivity in infants reveals altered connection strength associated with growth and preterm birth. Cerebral Cortex (in press).

Penfield W, Jasper HH (1954): Epilepsy and the functional anatomy of the human brain. Little Brown & Company, Boston.

Scheffer IE, Mullen SA (2013): Epilepsy in 2012: Advances in epilepsy shed light on key questions. Nat Rev Neurol 9:66–68.

Shannon P (2003): Cytoscape: A software environment for integrated models of biomolecular interaction networks. Genome Res 13:2498–2504.

Silberberg G, Markram H (2007): Disynaptic inhibition between neocortical pyramidal cells mediated by Martinotti cells. Neuron 53:735–746.

Smith SM (2002): Fast Robust Automated Brain Extraction. Hum Brain Mapp 17:143–155.

Strogatz SH (2001): Exploring complex networks. Nature 410:268–276.

Sugaya E, Goldring S, O'Leary JL (1964): Intracellular potentials associated with direct cortical response and seizure discharge in cat. Electroencephalogr Clin Neurophysiol 17:661–669.

Talairach J, Schaub C, Szikla G, Recoules D, Boujard O, Bleut-Pajot MT, Nassiet J, Lornet C (1974): Current indications of stereotaxic interstitial irradiation in acromegaly Ophthalmologic and neuroendocrinologic correlations in relation to prolonged time. Neurochirurgie 20:369–390.

Valentín A, Anderson M, Alarcón G, García Seoane JJ, Selway R, Binnie CD, Polkey CE (2002): Responses to single pulse electrical stimulation identify epileptogenesis in the human brain in vivo. Brain 125:1709–1718.

Valentín A, Alarcón G, Honavar M, García Seoane JJ, Selway RP, Polkey CE, Binnie CD (2005): Single pulse electrical stimulation for identification of structural abnormalities and prediction of seizure outcome after epilepsy surgery: A prospective study. Lancet Neurol 4:718–726.

van 't Klooster MA, Zijlmans M, Leijten FSS, Ferrier CH, van Putten MJAM, Huiskamp GJM (2011): Time-frequency analysis of single pulse electrical stimulation to assist delineation of epileptogenic cortex. Brain 134:2855–2866.

Varotto G, Tassi L, Franceschetti S, Spreafico R, Panzica F (2012): Epileptogenic networks of type II focal cortical dysplasia: A stereo-EEG study. Neuroimage 61:591–598.

Wiebe S, Jette N (2012): Pharmacoresistance and the role of surgery in difficult to treat epilepsy. Nat Rev Neurol 8: 669–677.

Wiebe S, Blume WT, Girvin JP, Eliasziw M (2001): A randomized, controlled trial of surgery for temporal-lobe epilepsy. N Engl J Med 345:311–318.

Wilke C, Worrell G, He B (2010): Graph analysis of epileptogenic networks in human partial epilepsy. Epilepsia 52:84–93.

Wilson CL, Isokawa M, Babb TL, Crandall PH (1990): Functional connections in the human temporal lobe I Analysis of limbic system pathways using neuronal responses evoked by electrical stimulation. Exp Brain Res 82:279–292.

Wilson CL, Khan SU, Engel JJ, Isokawa M, Babb TL, Behnke EJ (1998): Paired pulse suppression and facilitation in human epileptogenic hippocampal formation. Epilepsy Res 31:211–230.